A Lane Detection Algorithm Based on Reliable Lane Markings

Yasin YENİAYDIN, Klaus Werner SCHMIDT
Electrical and Electronics Engineering
Middle East Technical University
Ankara, Turkey
yeniaydin.yasin@metu.edu.tr, schmidt@metu.edu.tr

***Abstract*—This paper proposes a robust and effective vision-based lane detection approach. First, two binary images are obtained from the region of interest of gray-scale images. The obtained binary images are merged by a novel neighborhood AND operator and then transformed to a bird's eye view (BEV) via inverse perspective mapping. Then, gaussian probability density functions are fit to the left and right regions of a histogram image acquired from the BEV. Finally, a polynomial lane model is estimated from the identified regions. Experimental results show that the proposed method accurately detects lanes in complex situations including worn-out and curved lanes.**

Keywords — Vision-based lane detection; neighborhood AND operator; maximum likelihood estimation; parallelism of lanes.

I. INTRODUCTION

Advances in the field of autonomous and semi-autonomous vehicles such Lane Departure Warning (LDW) and Lane Keeping Assist System (LKAS) have a high potential to decrease the number of vehicle crashes [1, 2]. In order to realize LDW or LKAS, lane detection has to be performed, whereby vision-based lane detection is one of the main enablers for the lane detection [2, 3, 4, 5].

This paper develops a robust and effective vision-based lane detection approach. In the proposed method, gray-scale images are converted to two binary images from a fixed region of interest (ROI). These images are then merged using a novel neighborhood AND operator and then transformed to a bird's eye view (BEV) via inverse perspective mapping (IPM). A histogram image is extracted from the BEV and two gaussian probability density functions are fit to its left and right regions to determine the variance of the left and right lane markings. Finally, a polynomial lane model is estimated from the identified regions. Experimental results show that the proposed method accurately detects lanes in complex situations including worn-out and curved lanes. The novel neighborhood AND operator increases the robustness of the method.

The recent literature presents various lane detection methods. Similar to the proposed method, [6,7,8] suggest the usage of a fixed ROI. In [6], candidate lane pixels are detected by a 1-bit transform, feature points are determined by a Sobel filter and lane markings are detected based on the Hough Transform (HT). Lines are detected in binary images using a line segment detector and are then combined to lanes based on continuity information in [7]. Different from the proposed method, [6, 7, 9] do not use a BEV. [10] performs lane extraction based on complement Laplacian of Gaussian (cLog) and binary blob filtering after applying IPM. Lane detection is achieved using HT and the random sample consensus (RANSAC) algorithm. [8] performs feature extraction by a Step-Row filter and detects lanes using the HT. Different from the proposed method, [10] can eliminate the details of the lanes due to the performed image smoothing. A dynamic ROI is employed in [5, 10, 11]. Here, [3] proposes a fuzzy inference system to take into account shadows and performs lane detection based on a line segment detector. [11] uses a Sobel operator for feature extraction and detects lanes using the HT.

In addition to the stated particular differences between the proposed method and the existing approaches, it holds that the existing approaches mostly employ the HT for lane detection instead of the proposed polynomial lane model that makes use of the parallelism of lane markings. A notable exception is the work in [12] that develops a parallel snake lane model. Different from the proposed method, [12] does not consider focusing on the more reliable lane marking for lane detection.

The remainder of the paper is organized as follows. Section II gives background information and Section III develops the proposed method. Experimental results are presented in Section IV and Section V gives conclusions.

II. BACKGROUND

In this section, we summarize basic image processing techniques. We assume that images are given in RGB format and camera calibration has been performed [13].

Grayscale images carry enough information to detect lanes [2,3] and can be handled with smaller computational times. Hence, we convert the images in RGB format to grayscale format. Consider an RGB image as a map $I_{RGB}: M \times N \times \{R, G, B\} \rightarrow [0,1]$. $I_{RGB}(i, j, k)$ denotes the pixel value at row i, colum j for color k of the RGB image. M, N are the sets of rows, columns, respectively. Representing a grayscale image as a map $I_G: M \times N \rightarrow [0\ 1]$, an RGB image I_{RGB} is converted to a grayscale image I_G as follows [14]:

$$I_G(i,j) = 0.299\, I_{RGB}(i,j,R) + 0.587\, I_{RGB}(i,j,G) + 0.114\, I_{RGB}(i,j,B) \quad (1)$$

Sobel operators perform gradient measurements on grayscale images using convolution kernels for finding edges.

An example of 3x3 Sobel operators for finding vertical and horizontal lines are given as follows [15]:

978-1-5386-1501-0/18/$31.00 ©2018 IEEE

Vertical Line: $\begin{bmatrix}-1 & 0 & 1\\ -2 & 0 & 2\\ -1 & 0 & 1\end{bmatrix}$, Horizontal Line: $\begin{bmatrix}1 & 2 & 1\\ 0 & 0 & 0\\ -1 & -2 & -1\end{bmatrix}$

Global thresholding is used to binarize images for lane pixels in this work. A binary image $I_B: M \times N \rightarrow \{0,1\}$ is obtained from a grayscale image I_G as follows.

$$I_B(i,j) = \begin{cases} 1, & if\ I_G(i,j) \geq th \\ 0, & if\ I_G(i,j) < th \end{cases} \quad (2)$$

Here, $th \in [0,1]$ is a fixed threshold value.

Images are commonly obtained in a perspective view. To obtain a bird's eye view (BEV), we use the inverse perspective mapping (IPM) transformation [16]. It is formulated using the parameters in TABLE I.

TABLE I. PARAMETERS of BEV

Parameter	Description
P_i	Input pixel location
P_t	Transformed and scaled input pixel location
S, T	Scaling matrix, transformation matrix
u, v	Column/row index of the output pixel
N_c, N_r	number of columns/rows of the image
f	focal length of the camera

Rotation and translation of the pixel locations are performed by the transformation matrix T, whose parameters are chosen for a top-down view. The scaling matrix S stretches the image in height since the image shrinks in height after rotation. Lastly, the output pixel location is represented by u and v after projecting the coordinates (p, q, r) of P_t in 3D to 2D with the help of the focal length of the camera.

$$P_t = S \cdot T \cdot P_i \quad (3)$$

$$u = \frac{f\,p}{f-r} + \frac{N_c}{2} \quad \text{and} \quad v = \frac{f\,q}{f-r} + \frac{N_r}{2} \quad (4)$$

$$P_t = \begin{bmatrix} p \\ q \\ r \\ 1 \end{bmatrix}, S = \begin{bmatrix} s_x & 0 & 0 & 0 \\ 0 & s_y & 0 & 0 \\ 0 & 0 & 1 & 0 \\ 0 & 0 & 0 & 1 \end{bmatrix}, T = \begin{bmatrix} r_{11} & r_{12} & r_{13} & -\frac{N_c}{2} \\ r_{21} & r_{22} & r_{23} & -\frac{N_r}{2} \\ r_{31} & r_{32} & r_{33} & 0 \\ 0 & 0 & 0 & 1 \end{bmatrix}, P_i = \begin{bmatrix} i \\ j \\ 0 \\ 1 \end{bmatrix}$$

Polynomials are one possible lane model [2]. To find parameters of such lane model based on measurements, the least-square error (LSE) method is suitable [17]. Consider a set of N measurement pairs $\{(i_1, j_1), (i_2, j_2), \ldots, (i_N, j_N)\}$ and a second order polynomial

$$ai^2 + bi + c = j \quad (6)$$

Then, the LSE formulation determines a, b, c as

$$\bar{x} = (A^T A)^{-1} A^T \bar{j} \quad (7)$$

With the matrices and vectors

$$A = \begin{bmatrix} {i_1}^2 & i_1 & 1 \\ {i_2}^2 & i_2 & 1 \\ \vdots & \vdots & \vdots \\ {i_N}^2 & i_N & 1 \end{bmatrix}, \bar{x} = \begin{bmatrix} a \\ b \\ c \end{bmatrix}, \bar{j} = \begin{bmatrix} j_1 \\ j_2 \\ \vdots \\ j_N \end{bmatrix},$$

thus minimizing the squared error vector

$$e = \|A\bar{x} - j\|_2^2 = (A\bar{x} - \bar{j})^T (A\bar{x} - \bar{j}) \quad (8)$$

III. PROPOSED METHOD

A. Overview

The proposed method comprises four steps that are summarized in Figure 1. First, the region of interest (ROI) is defined and feature extraction on binary images is performed via a novel neighborhood AND operator. Second, BEV is obtained using the IPM. Third, the lane detection region (left or right) is computed based on the distribution of lane pixels on the BEV. Lastly, the parameters of the lane model are computed using the LSE method.

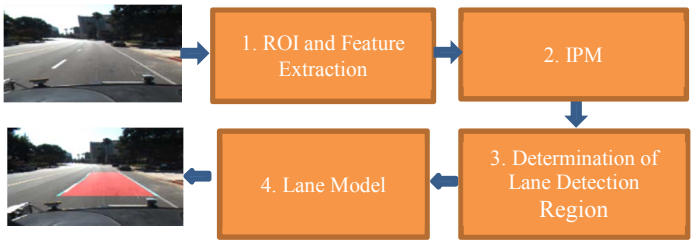

Figure 1. Block diagram of the proposed method.

B. Detailed Steps of the Method

Step 1) The undistorted RGB image after calibration is first converted to a grayscale image as in (1). After that, to focus on the lanes and to reduce the image processing time, the ROI is selected on grayscale image. Then, two binary images I_{B1} and I_{B2} are acquired, applying (2) to (i) the grayscale image I_G itself and (ii) to the gradient magnitude image after applying the Sobel operator in Section II to I_G.

The binary images are then merged via the novel neighborhood AND operator in (9) with the proximity parameter k.

$$I(i,j) = \begin{cases} 0 & \text{if } \left(\sum_{l=i-k}^{i+k}\sum_{m=j-k}^{j+k} I_{B1}(l,m)\right) \cdot \left(\sum_{l=i-k}^{i+k}\sum_{m=j-k}^{j+k} I_{B2}(l,m)\right) = 0 \\ 1 & \text{otherwise} \end{cases} \quad (9)$$

(9) determines $I(i,j) = 0$ if all neighboring pixels in a square with $k \cdot k$ pixels are zero for both I_{B1} and I_{B2}. Otherwise, $I(i,j) = 1$. As a result of this operation, we expect that the ones of the resulting binary image I represent the lane markings (white) and all remaining parts of the image are zero (black). The proposed neighborhood AND operator makes common features in a close vicinity more concrete and discards non-shared features. The parameter k is determined experimentally in this work.

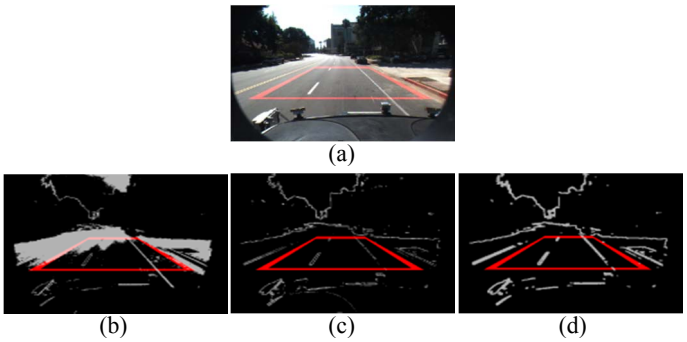

Figure 2. (a) Image in RGB format; binary image obtained (b) in Step 2-(i), (c) in Step 2-(ii), (d) after neighborhood AND.

In Figure 2, binary images obtained from an RGB image are shown and the areas in the red trapezoids indicate the ROI. The original RGB image which is taken from the CalTech database [18] is given in Figure 2(a). The binary images obtained in Step

1-(i) and Step 1-(ii) are shown in Figure 2(b-c), respectively. Figure 2(d) displays the final binary image after applying neighborhood AND. Note that, (9) is applied to the complete image (and not only to the ROI) for illustration.

As can be seen from Figure 2(d), neighborhood AND indeed strengthens the common features of Figure 2(b-c). Hereby, the application of the Sobel operator helps discarding parts of Figure 2(b) with low contrast, whereby the usage of Figure 2(b) makes the detected lanes more concrete.

Step 2) To make use of the parallelism of the lanes, the images are transformed to the BEV via IPM. In Figure 3(a-b), BEVs of Figure 2(a) and Figure 2(d) are given, respectively.

(a) (b)

Figure 3. BEV in RGB (a) and binary (b) formats.

Step 3) We next determine regions on the binary BEV that should be used for lane detection. Firstly, a histogram plot of the binary BEV along the x-axis is obtained. The y-axis represents the number of candidate lane pixels for each column of the binary BEV. In Figure 4, the histogram plot of the binary image for Figure 3(b) is given and is divided in a left and right region with respect to the vehicle center. Since the proximity of lane pixels to each other play an important role for a good lane detection, standard deviations σ_l, σ_r by using mean values μ_l, μ_r on the left (l) and right (r) region of the histogram plot are computed. To determine the parameters, we fit a Gaussian probability density function (pdf) to the candidate lane pixels in the left and right regions via maximum likelihood estimation (MLE):

$$\mu_{\mathrm{l}} = \frac{2}{N}\sum_{\mathrm{j}=1}^{\mathrm{N}/2}\sum_{i=1}^{M} j \cdot I(i,j);\ \sigma_l^2 = \frac{2}{N}\sum_{\mathrm{j}=1}^{\mathrm{N}/2}\sum_{i=1}^{M} \mathrm{I(i,j)} \cdot (\mathrm{j} - \mu_l)^2 \qquad (10)$$

$$\mu_{\mathrm{r}} = \frac{2}{N}\sum_{\mathrm{j}=\mathrm{N}/2+1}^{\mathrm{N}}\sum_{i=1}^{M} j\, I(i,j);\ \sigma_r^2 = \frac{2}{N}\sum_{\mathrm{j}=\mathrm{N}/2+1}^{\mathrm{N}}\sum_{i=1}^{M} \mathrm{I(i,j)}(\mathrm{j} - \mu_r)^2 \qquad (11)$$

Figure 5 shows the MLE results for Figure 3(b).

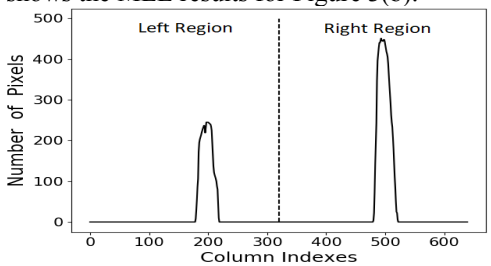

Figure 4. Histogram plot representing distribution of candidate lane pixels on the BEV and showing the left and right regions.

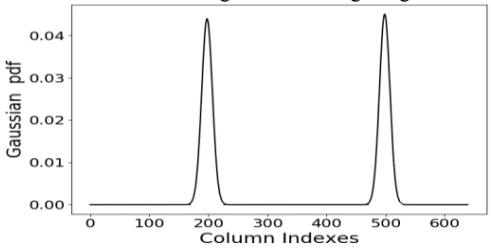

Figure 5. MLE results of candidate lane pixels in left/right regions.

In this paper, we propose to perform the lane detection using the most reliable lane. The criterion to determine which region is selected for the lane detection is as follows:

$$\text{Choose left region, if } (t\ P_{\mathrm{l}} - \sigma_{\mathrm{l}}) \geq (t\ P_{\mathrm{r}} - \sigma_{\mathrm{r}})$$

$$\text{Choose right region, if } (t\ P_{\mathrm{l}} - \sigma_{\mathrm{l}}) < (t\ P_{\mathrm{r}} - \sigma_{\mathrm{r}}) \qquad (12)$$

In (12), P_{l}, P_{r} denote the peak values in the left/right region of the histogram and t is a trade-off parameter between peak value and standard deviation. The proposed criterion determines the more distinctive peak, whereby more importance can be given to the peak value or the standard deviation by t. In this work, t is determined experimentally.

Step 4) Up to this point, we found the column index of P_{l} or P_{r} as the basic location of the lane marking to be detected. In this step, we precisely determine the shape of the lane pixels along the column indexes by scanning the BEV row by row (respecting the fact the lane might be curved). This step is visualized in Figure 6, where the right region was selected for lane detection based on (12). Intuitively, the red rectangles scan the BEV from bottom to top along the y-axis. The x-position of each red rectangle is determined by the mean of the x-coordinates of the lane pixels in the respective previous rectangle starting from column index of P_{r}. In this work, the height h and width w of the rectangle are fixed experimentally. The parameters of the polynomial in (6) for the detected lane are finally computed by applying the LSE method to all the pixels covered by red rectangles. The computed lane polynomial is then shifted to the column position of the peak value in the other region to obtain the second lane marking.

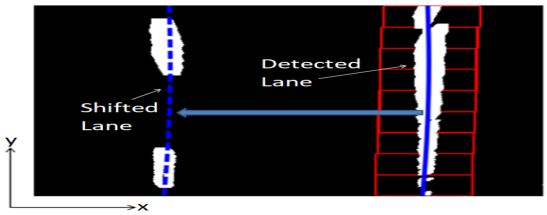

Figure 6. Visualization of the lane detection.

IV. EXPERIMENTAL RESULTS

To evaluate the proposed algorithm, we used images from [18]. TABLE II shows the selected parameter values.

TABLE II. PARAMETER VALUES.

Parameter	Value	Parameter	Value
k	2	t	5
Threshold in Step 2-(i)	0.59	h	54
Threshold in Step 2-(ii)	0.29	w	50

In the experiments, the tradeoff parameter $t = 5$ is chosen, giving more importance to the number of lane pixels in one column than to the standard deviation of the lane pixels for achieving an accurate lane detection. A representative selection of lane detection results is given in Figure 7.

As can be seen from Figure 7(a-b-c), our algorithm detects lanes which are in a good condition. Even if there are signs close to the lane, it performs well. Further, the proposed method can detect the lane in complex cases such as lanes that are affected by shadows and occupied by other vehicles as can be seen in Figure 7(d-e-f). Moreover, we evaluated the algorithm with only one lane and when the road has different colors of asphalt as in Figure 7(g). In addition to that, the

result of correct detection for worn-out and non-parallel lanes are shown in Figure 7(h). More than that, we can see a correct detection when the road is curved as in Figure 7(i). Lastly, there can exist different signs on top of lanes especially in urban streets. Examples of those situations and the results of correct lane detections are given in Figure 7(j-k-l).

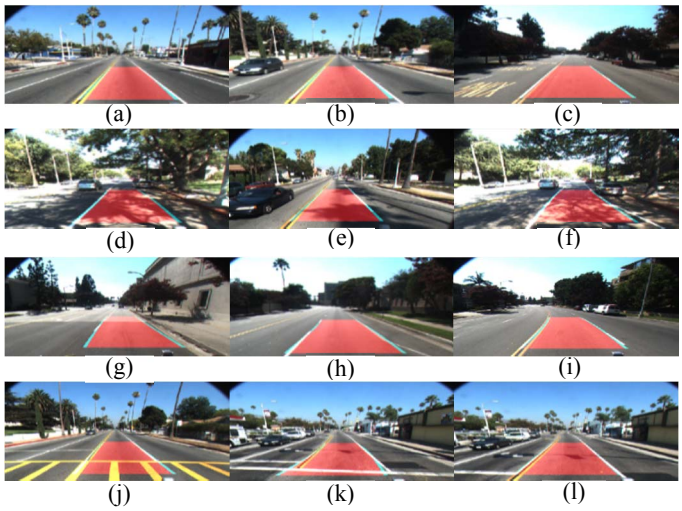

Figure 7. Experimental lane detection results.

For quantitative results, we compare neighborhood AND with different feature extraction methods in the same ROI of the images in [18] that were manually labeled for solid and dashed lanes. F-measure, precision and recall metrics as in (13) are used. The number of true positives, false positives and false negatives are represented as #TP, #FP, #FN, respectively.

$$Pre = \frac{\#TP}{\#TP + \#FP}, \quad Re = \frac{\#TP}{\#TP + \#FN}, \quad F = \frac{2 \cdot Pre \cdot Re}{Pre + Re} \tag{13}$$

Precision indicates the noise removal of the method, recall shows the ratio of extracted lane pixels over all lane pixels. The F-measure combines the precision and recall and it is high when the precision and recall are both high.

The average results of the metrics are given in TABLE III.

TABLE III. Results for Feature Extraction (Cordova1 Dataset in [18]).

Feature Extraction Methods	Precision	Recall	F-measure
Neighborhood AND	0.788	0.816	0.782
1-Bit Transform [6]	0.892	0.354	0.490
Feature Extraction in [9]	0.615	0.474	0.522
Feature Extraction in [18]	0.577	0.741	0.645

The quantitative results support the effectiveness of the proposed neighborhood AND operator.

V. CONCLUSIONS

This paper proposes a robust lane detection method under the assumption that lane markings are parallel. Experiments show that detecting the more reliable lane marking and estimating the other one performs very well even in complex conditions. Since the algorithm only performs basic operations on gray-scale images and uses least-square error and maximum likelihood estimation methods on histogram plots, it has a high potential for real time applications. In the future, we intend to extend the algorithm by lane tracking.

ACKNOWLEDGMENT

This work is supported by the Middle East Technical University Research Project BAP-03-01-2018-008.

REFERENCES

[1] I. J. Reagan, J. B Cicchino, L. B. Kerfoot, and R. A. Weast, “Crash avoidance and driver assistance technologies – Are they used?”, Transportation Research Part F: Traffic Psychology and Behaviour, vol. 52, pp. 176-190, 2018.

[2] S. P. Narote, P. N. Bhujbal, A. S. Narote, and D. M. Dhane, “A review of recent advances in lane detection and departure warning system”, Pattern Recognition, vol. 73, pp. 216-234, 2018.

[3] T. M. Hoang, N. R. Baek, S. W. Cho, K. W. Kim, and K. R. Park, “Road lane detection robust to shadows based on a fuzzy system using a visible light camera sensor”, Sensors, vol. 17(11), pp. 2475, 2017.

[4] C. Bila, F. Sivrikaya, M. A. Khan, and S. Albayrak, “Vehicles of the Future: A Survey of Research on Safety Issues”, IEEE Transactios on Intelligent Transportation Systems, vol. 18(5), pp. 1046-1065, 2017.

[5] A. Mammeri, G. Lu, A. Boukerche, "Design of lane keeping assist system for autonomous vehicles", 2015 7th International Conference on New Technologies Mobility and Security (NTMS), pp. 1-5, July 2015.

[6] A. Küçükmanisa, R. Duvar, and O. Urhan, “Real-Time Lane Marking Detection using Modified 1-Bit Transform based Pre-processing”, 25th Signal Processing and Communications Applications Conf., pp. 1-4, 2017.

[7] J. Duan, Y. Zhang, B. Zheng, “Lane Line Recognition Algorithm Based on Threshold Segmentation and Continuity of Lane Line”, 2nd IEEE International Conference on Computer and Communications, pp. 680-684, 2016.

[8] R. F. Berriel, E. D. Aguiar, A. F. D. Souza, T. O. Santos, “Ego-Lane Analysis System (ELAS): Dataset and algorithms”, Image and Vision Computing, vol. 68, pp. 64–75, 2017.

[9] U. Ozgunalp, N. Dahnoun, “Robust lane detection amp; tracking based on novel feature extraction and lane categorization”, Accoustic Speech and Signal Processing (ICASSP) 2014 IEEE International Conference on, pp. 8129-8133, May 2014.

[10] J. Piao, H. Shin, “Robust hypothesis generation method using binary blob analysis for multi-lane detection”, IET Image Process., vol. 11(12), pp. 1210-1218, 2017.

[11] K. Manoharan, P. Daniel, “Image processing-based framework for continuous lane recognition in mountainous roads for driver assistance system”, J. Electron. Imaging, vol. 26(6), pp. 063011, 2017.

[12] Li Xiangyang et al., “Lane detection and tracking using a parallel-snake approach”, Journal of Intelligent & Robotic Systems, vol. 77(3-4), pp. 597–609, 2015.

[13] Z. Zhang, “A flexible new technique for camera calibration”, IEEE Trans. Pattern Analysis and Machine Intelligence, vol. 22(11), pp. 1330–1334, 2000.

[14] C. Saravanan, “Color Image to Grayscale Image Conversion”, Computer Engineering and Applications (ICCEA) 2nd International Conf., pp. 196-199, 2010.

[15] G. Chaple, R.D. Daruwala, "Design of Sobel operator based image edge detection algorithm on FPGA", International Conference on Communications and Signal Processing (ICCSP), pp. 788-792, 2014.

[16] M. Venkatesh and P. Vijayakumar, "A simple bird's eye view transformation technique", Int. J. Sci. & Eng. Research, vol. 3(5), pp. 735-738, 2012.

[17] J. Son, H. Yoo, S. Kim, K. Sohn, “Real-time illumination invariant lane detection for lane departure warning system”, Expert Syst. Appl., vol. 42(4), pp. 1816–1824, 2015.

[18] M. Aly, “Real time detection of lane markings in urban streets”, Proc. IEEE Intell. Vehicles Symp., pp. 7-12, 2008.